The magnetocaloric effect of the lanthanide fluorides: Using polarized neutron scattering to probe a magnetocaloric suitable for hydrogen liquefaction

Richard J. C. Dixey, Andrew Wildes, Patrick W. Doheny, Gavin B. G. Stenning, and Paul J. Saines

Published version information

Citation: RJC Dixey et al. The magnetocaloric effect of the lanthanide fluorides: Using polarized neutron scattering to probe a magnetocaloric suitable for hydrogen liquefaction. APL Mater 11, no. 4 (2023): 041126

DOI: 10.1063/5.0139726

RESEARCH ARTICLE | APRIL 19 2023

The magnetocaloric effect of the lanthanide fluorides: Using polarized neutron scattering to probe a magnetocaloric suitable for hydrogen liquefaction

Special Collection: Challenges and Perspectives in Materials Chemistry—A Celebration of Prof. Sir Anthony K. Cheetham's 75th Birthday

Richard J. C. Dixey; Andrew Wildes; Patrick W. Doheny; ... et. al

APL Mater 11, 041126 (2023)
https://doi.org/10.1063/5.0139726

The magnetocaloric effect of the lanthanide fluorides: Using polarized neutron scattering to probe a magnetocaloric suitable for hydrogen liquefaction

Cite as: APL Mater. 11, 041126 (2023); doi: 10.1063/5.0139726
Submitted: 22 December 2022 • Accepted: 23 March 2023 •
Published Online: 19 April 2023

Richard J. C. Dixey,[1] Andrew Wildes,[2] Patrick W. Doheny,[3] Gavin B. G. Stenning,[4] and Paul J. Saines[3,a)]

AFFILIATIONS

[1]Centre for Condensed Matter, Queen Mary University of London, London E1 4NS, United Kingdom
[2]Institut Laue-Langevin, CS 20156, 38042 Grenoble Cedex 9, France
[3]School of Chemistry and Forensic Science, Ingram Building, University of Kent, Canterbury CT2 7NH, United Kingdom
[4]ISIS Facility, STFC Rutherford Appleton Laboratory, Chilton, Didcot OX11 0QX, United Kingdom

Note: This paper is part of the Special Topic on Challenges and Perspectives in Materials Chemistry - A Celebration of Prof. Sir Anthony K. Cheetham's 75th Birthday.
[a)]**Author to whom correspondence should be addressed:** P.Saines@kent.ac.uk

ABSTRACT

This work reports the competitive magnetocaloric effect of some simple lanthanide fluoride materials with cations with high magnetic anisotropy. Of these, HoF_3 is particularly promising due to exhibiting a high magnetocaloric entropy change under modest applied fields at higher temperatures, which only decreases modestly with temperature such that it has the potential for cooling for hydrogen liquefaction. Spin-polarized neutron spectroscopy indicates that its promising conventional magnetocaloric effect is likely due to the presence of ferromagnetic fluctuations of highly anisotropic magnetic moments, while its singlet electronic ground state and low-temperature magnetic ordering lead to a decrease in its magnetocaloric performance below 4 K.

I. INTRODUCTION

The magnetocaloric effect (MCE) is an energy-efficient and environmentally friendly alternative to vapor compression refrigeration technology, with superior theoretical energy efficiencies of >50% compared to ~35% for vapor compression.[1,2] While magnetocalorics have historically been optimized for ultra-low temperature (< 2 K), they have recently been considered suitable as a replacement for liquid helium refrigeration or liquefaction of hydrogen gas (< 20 K) as promising MCE at higher temperatures is achieved.[3,4] The MCE arises from the change in entropy when a magnetic field is applied and then removed from a paramagnetic material. The initial application of a magnetic field causes the spins to align with the external magnetic field, producing a more ordered state thereby reducing the magnetic entropy of the system. This results in a positive adiabatic temperature change (ΔT_{ad}) as the total magnetic entropy of the system approaches zero. This heat is subsequently removed from the system while the field is still applied, and when the field is removed, the entropy of the system increases and a negative ΔT_{ad} results. This cooling process can be iterated to lower the temperature of the material; however, for this effect to work optimally, the material must remain paramagnetic over the working temperature range.

The need for dense magnetocalorics with high magnetic moments has driven an interest in MCE materials based on the later lanthanides owing to the high magnetic entropy change (ΔS_m) they support. A new wave of non-oxide magnetocalorics has been recently reported to have particularly high magnetocaloric effects,

including $Gd(HCO_2)_3(C_2O_4)$, $GdPO_4$, $Gd(HCO_2)_3$, $GdOHCO_3$, and GdF_3, which have superior performance to the benchmark $Gd_3Ga_5O_{12}$ (GGG) phase.[5–10] Recent work has shown the substitution of Gd for other lanthanide ions with Ising-like spins leading to a larger $-\Delta S_m$ above 2 K in low applied fields,[11–14] at the expense of a slight decrease in the performance for larger field changes. Achieving magnetocaloric materials optimized for higher temperatures and, ideally, the more modest applied fields that can be generated using a permanent magnet (less than 2 T), offers the potentially high-efficiency cryogen-free cooling technology for a wider range of applications. This has inspired the study of analogs of promising Gd magnetocalorics containing other magnetically anisotropic lanthanides.

The benefits of exploring magnetocalorics with magnetically anisotropic cations have already been highlighted by studies of the $Ln(HCO_2)_3$ (Ln = Gd^{3+}, Tb^{3+}, Dy^{3+}, Ho^{3+}, and Er^{3+}) series, which have shown that $Tb(HCO_2)_3$ has higher $-\Delta S_m$ than $Gd(HCO_2)_3$ above 4 K and field changes below 2 T.[11] Similarly, among the $LnOHCO_3$ phases, $TbOHCO_3$ and $DyOHCO_3$ have higher $-\Delta S_m$ than $GdOHCO_3$ above 4 K for similarly modest field changes.[12] Previous studies on these two families have shown that the reason these materials can stay paramagnetic in their magnetocaloric operating temperatures is due to significant frustration between neighboring chains of spins that are arranged in triangular motifs and stacked into layers forming chains of magnetic ions.[11,15–18] These Ising-like spin chains also possess strong intrachain ferromagnetic correlations, which allow for easy alignment of the spins with the magnetic fields once the antiferromagnetic correlations are overcome.

The LnF_3 family of materials crystallize in the orthorhombic $Pnma$ space group (a = 6.40, b = 6.87, and c = 4.38 Å for HoF_3 at room temperature).[19] The structure can be viewed as having chains of LnF_9 face-sharing polyhedra, with corner-sharing interchain connectivity. Intrachain nearest neighbor Ho^{3+} are separated by 3.6 Å, with the next nearest neighbor interchain distance of 4.1 Å. The LnF_3 phases have similar structural characteristics to the $Ln(HCO_2)_3$ and $LnOHCO_3$ phases, with their chains packed into distorted triangular lattices (see Fig. 1). GdF_3 is reported to have the highest $-\Delta S_m{}^{max}$, and therefore, we have chosen to investigate the magnetocaloric effect in the LnF_3 family of materials.[8] We find that HoF_3 has significantly higher $-\Delta S_m$ than GdF_3 at low fields above 4 K, with a slow decrease in the performance being particularly impressive, enabling it to retain high $-\Delta S_m$ well above 10 K. This makes it useful for cooling over a significantly broader range of temperatures, and, therefore, applications, than is typical for a magnetocaloric, including cooling to near 20 K for hydrogen liquefaction. Below 4 K, the $-\Delta S_m$ of HoF_3 decreases significantly, leading to an apparent inverse MCE at 2 K. This is attributed to a combination of its, previously reported, singlet electronic ground state and low temperature canted antiferromagnetic order.[20,21]

II. EXPERIMENTAL METHODS

Polycrystalline samples of LnF_3 (Ln = Gd^{3+}, Tb^{3+}, Dy^{3+}, Ho^{3+}, and Er^{3+}) were purchased from Fisher Scientific and used without any further purification. Sample phase purity was examined by powder X-ray diffraction measurements performed on ground polycrystalline samples on a Rigaku MiniFlex with CuK_α radiation using a zero-background silicon sample holder. The X-ray powder patterns were refined using the FULLPROF suite employing the Pawley fitting method and a linear background of interpolated points (see Figs. S1–S5 for the resulting fits), which indicated that only DyF_3 contained a small unknown impurity.[22]

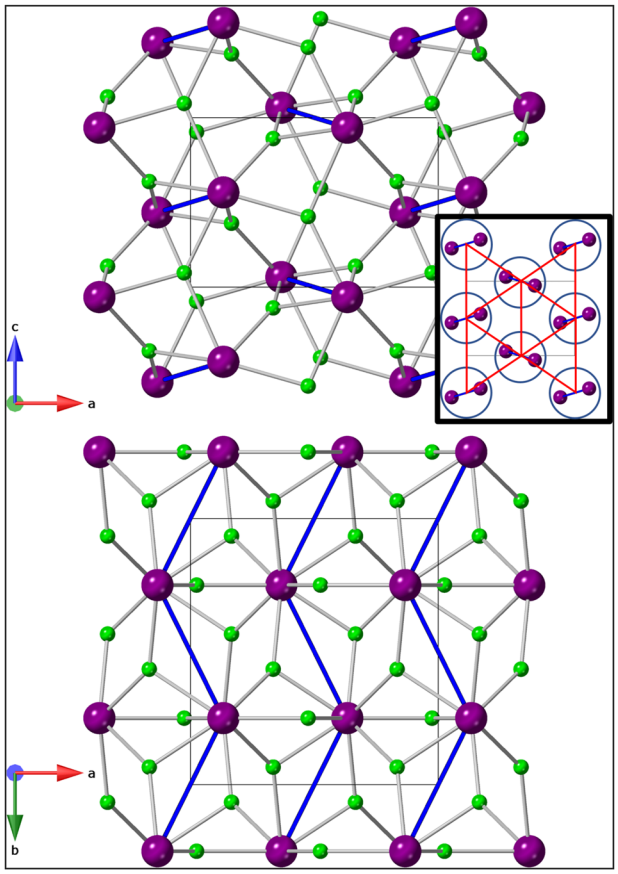

FIG. 1. Two diagrams of the isostructural LnF_3 materials oriented along the b and c axes. Ln^{3+} are shown in purple and F are shown in green. The nearest neighbor interactions are shown as blue rods. The top diagram oriented along the b axis shows the triangular motifs in the insert, between buckled spin chains, and the bottom diagram shows the nearest neighbor interactions forming chains of Ln^{3+} atoms. Crystal structure data are taken from Piotrowski *et al.*[19]

The magnetic measurements of the polycrystalline samples (15–20 mg) were performed using a Quantum Design MPMS SQUID magnetometer. The samples were placed in gelatin capsules enclosed inside a pierced straw with a uniform diamagnetic background. Zero field cooled (ZFC) and field cooled (FC) measurements were recorded in a DC field between 2–300 K for LnF_3 (where Ln = Gd-Er) in a 1000 Oe applied field. Field sweeps used to calculate ΔS_m using Maxwell relations were measured in a DC field and magnetic fields of 0–5 T, with varying intervals.

Powder neutron scattering measurements were carried out on the D7 diffuse scattering spectrometer in both diffraction and inelastic modes using the neutron reactor source at the Institut Laue-Langevin, Grenoble, France.[23] A sample of 7.977 g of polycrystalline HoF_3 was ground in a pestle and mortar and loaded into an aluminum can, which had a 20 mm inner diameter with a 19 mm

insert to give the sample an annular cross-section. The experiment used polarized neutrons with a wavelength of 3.1327 Å and incident energy equal to 8.34 meV from the pyrolytic graphite (002) monochromator. The neutrons were polarized and analyzed using supermirror benders, with a precession-coil spin flipper in the incident beam and current-carrying coils around the sample to control the polarization direction. The XYZ polarization analysis method, involving the linear combinations of the measured non-spin–flip and spin–flip intensities for the polarization along three orthogonal directions,[23] was used to separate the nuclear coherent, nuclear spin-incoherent, and magnetic scattering signals from the total scattering. Diffraction measurements were carried out between 1.5 and 150 K. A Fermi chopper was then placed between the monochromator and the sample for spectroscopic measurements at 1.5 K, permitting the final neutron energy to be determined from the time-of-flight between the sample and the detectors.

III. RESULTS AND DISCUSSION

A. Magnetic properties

Field cooled (FC) and zero-field cooled (ZFC) magnetic susceptibility data of the LnF_3 frameworks (Ln = Gd^{3+}, Tb^{3+}, Dy^{3+}, Ho^{3+}, and Er^{3+}) were measured in a 1000 Oe field from 2 to 300 K. The magnetic susceptibility data for all LnF_3 were found to obey the Curie–Weiss law between 100 and 300 K (Figs. S6–S10). The effective magnetic moments were found to be broadly consistent with the values expected for these trivalent lanthanides according to the Russell–Saunders coupling scheme[24] (see Table I). The Curie–Weiss temperatures, θ_{CW}, of Ln = Tb-Er indicate predominantly antiferromagnetic interactions within these materials, although this must be interpreted carefully due to likely contributions from crystal field effects of the Ln cations at low temperatures.

Extrapolation of the Curie–Weiss fits above 100 K to lower temperatures for GdF_3, DyF_3, HoF_3, and ErF_3 did not show any indication of the deviation from purely paramagnetic behavior down to 2 K (see Figs. S6 and S8–S10). In contrast, TbF_3 was found to deviate from the Curie–Weiss law below 2.9 K with $\chi_M T$ also increasing rapidly at low temperatures, with a maximum observed at ~3 K (see Figs. S7 and S11). A weak divergence of ZFC and FC magnetic susceptibilities is also observed at this temperature and reflects the onset of this long-range magnetic order. This is in broad agreement with the onset of magnetic order reported in TbF_3 at ~3.97 K, consisting of canted Ising-spin magnetic order.[25,26]

TABLE I. Curie–Weiss temperatures and effective magnetic moments for lanthanides in LnF_3.

Ln	θ_{CW} (K)	Curie constant (emu mol^{-1} Oe^{-1})	Magnetic moment (μ_B)
Gd	0.42	7.32	7.65
Tb	−4.74	10.81	9.30
Dy	−4.69	12.79	10.11
Ho	−11.56	15.71	11.21
Er	−11.59	11.44	9.56

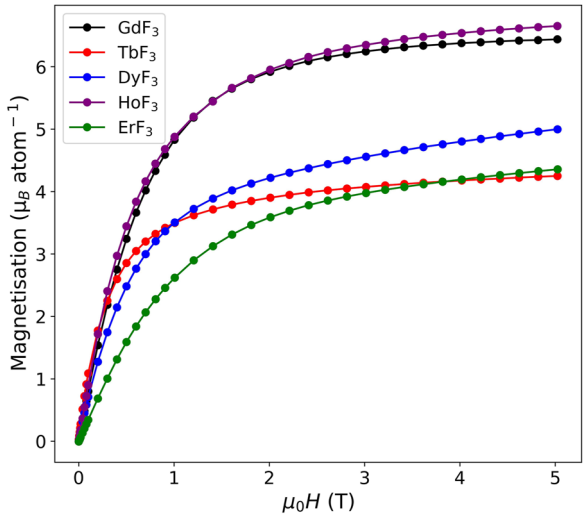

FIG. 2. Isothermal magnetization measurements of the LnF_3 series measured at 2 K.

Isothermal magnetization measurements on the LnF_3 frameworks measured at 2 K (Fig. 2) reveal that only GdF_3 has magnetization consistent with a Heisenberg spin, approaching 7 μ_B under high applied magnetic fields. In contrast, TbF_3, DyF_3, and ErF_3 all show saturation values close to that of $g_J J/2$ expected for purely Ising anisotropy[27–30] and materials with large spin–orbit coupling. Finally, HoF_3 shows a steep magnetization in low applied fields and saturates at values close to, but noticeably exceeding, the limit expected for the magnetic cations in an Ising case, which may suggest that it exhibits high magnetic anisotropy deviating from purely Ising behavior. This is analogous to the effect we have reported in $DyOHCO_3$,[17] which showed the most promising ΔS_m at elevated temperatures among the LnOHCO$_3$ phases.[12,15,17] The magnetization of GdF_3, TbF_3, and HoF_3 show a steep rise in magnetization with all nearing plateaus below 2 T. At 2 K, none of this series shows hysteresis in the magnetization.

B. Magnetocaloric effects

$-\Delta S_m$ values were calculated using the Maxwell relation [see Eq. (1)] between 2 and 10 K, and for field changes between 0 and 1–5 T (see Fig. 3 for 0–1 and 0–2 magnetocaloric effect plots, Figs. S12–S14 for 0–3, 0–4, and 0–5 T field changes, and Figs. S15–S20 for magnetization plots from which these values are obtained). The Maxwell relation used for calculating the magnetic entropy changes (ΔS_m) at a given temperature is shown as follows:

$$\Delta S_m = \int \left[\frac{\delta M_{T,\mu_0 H}}{\delta T}\right]_{\mu_0 H} d\mu_0 H, \quad (1)$$

where T is the absolute temperature, M is magnetization at a given temperature and applied magnetic field, and $\mu_0 H$ is the applied magnetic field.

As expected from other lanthanide magnetocaloric materials, the previously reported GdF_3 is observed to have the greatest $-\Delta S_m^{max}$ at 2 K, particularly in multiple Tesla magnetic fields. For moderate field changes of less than 2 T, TbF_3 and HoF_3 are found to

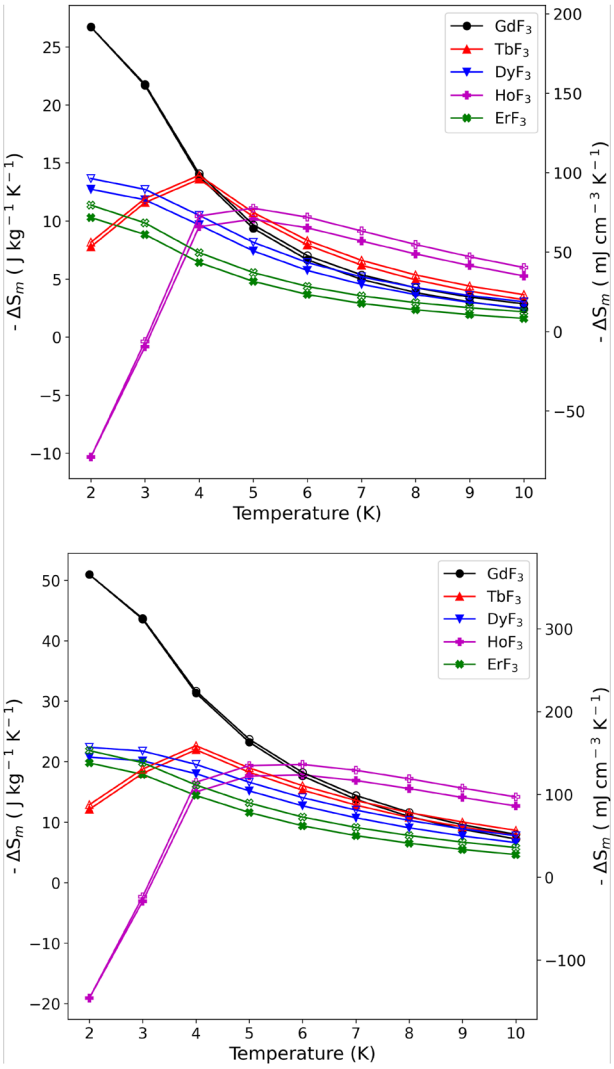

FIG. 3. The magnetocaloric effects of the LnF_3 materials for $\Delta\mu_0 H$ = 0–1 T (top) and 0–2 T (bottom). The filled and hollow symbols mark mass and volumetric units, respectively.

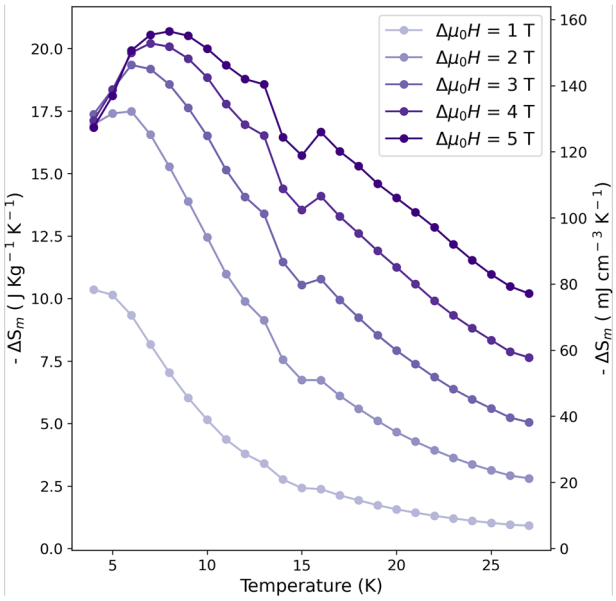

FIG. 4. The magnetocaloric effect of HoF_3 in magnetic field changes between 1 and 5 T plotted in mass and volumetric units.

perform well with $-\Delta S_m{}^{max}$ at 4 and 6 K, with HoF_3 outperforming GdF_3 above 5 K with a very gradual decrease suggesting that this differential will increase significantly at higher temperatures. The slow, almost linear, decline of $-\Delta S_m$ with respect to temperature in these initial studies inspired further investigation into the magnetocaloric effect of HoF_3 to higher temperatures.

As shown in Fig. 4, magnetisation measurements enable the magnetocaloric entropy change for HoF_3 to be determined up to 27 K, where we observe excellent magnetocaloric behavior in applied field changes of between 2 and 5 T. An anomalous reduction in the magnetocaloric effect is observed in HoF_3 in higher fields changes at 14 and 15 K. A summary of the peak MCE temperatures of all the LnF_3 is given in Table II, showing the temperatures at which the MCE peaks in both mass and volumetric units with regard to the performance above 4 K. Due to the high density of the LnF_3 materials, HoF_3 outperforms other similar materials, when comparing volumetric units, above 8 K.[12,16,31–33]

Notably, the $-\Delta S_m$ values of HoF_3 decrease significantly below 4 K with an apparent inverse magnetocaloric effect at 2 K. From the Maxwell relation, this can be interpreted as indicating a decrease in the magnetization with decreasing temperature ($\delta M/\delta T$) as is observed in the magnetization data. This observation should be interpreted carefully as it relies heavily on the 2 K magnetization measurement and requires further studies to confirm that this is not an experimental artifact. If confirmed, this is consistent with the material being close to a magnetic anomaly. A secondary interesting feature of HoF_3 is the field dependence of the peak temperature of the magnetocaloric effect. It appears that with larger changes in the magnetic field, the temperature at which the magnetocaloric effect peaks increases significantly, which has been observed in other highly anisotropic holmium-containing polycrystals.[34] HoF_3 has interesting properties compared to the benchmark GGG and DGG materials. For ΔB = 0–2 T, GGG has a $-\Delta S_m{}^{max}$ = 17.7 J kg^{-1} K^{-1} or 145 mJ cm^{-3} K^{-1} at 1.2 K,[33] and DGG has a $-\Delta S_m{}^{max}$ = 11.64 J kg^{-1} K^{-1} or 95 mJ cm^{-3} K^{-1} at 1.2 K.[13,27,35] HoF_3 shows an entropy change of 17.80 J kg^{-1} K^{-1} or 136.12 mJ cm^{-3} K^{-1} at 5 K for the same field change, and even at 12 and 16 K, it has an entropy change of greater than 10 J kg^{-1} K^{-1} or 50 mJ cm^{-3} K^{-1}.

HoF_3 has a $-\Delta S_m{}^{max}$ of 21.22 J kg^{-1} K^{-1} for a field change of 0–5 T and retains a value of larger than 14.02 J kg^{-1} K^{-1} up to 20 K, the boiling point of hydrogen, for a 0–5 T field change. This compares favorably to the mineral Gaudefroyite, which has been previously touted for use as a magnetocaloric for hydrogen liquefaction based on a $-\Delta S_m{}^{max}$ of less than 15 J kg^{-1} K^{-1} and retaining a value of above 10 J kg^{-1} K^{-1} up to 20 K for a similar field change.[4,36] This gives commercially available HoF_3 the potential to find uses

TABLE II. Summary of the peak MCE ($-\Delta S_m^{max}$) at peak temperatures [T_{max} (K)] of the studied LnF_3 at different field changes. Mass refers to changes in entropy per mass in units of J kg^{-1} K^{-1}, and volume refers to change in entropy per volume in units of mJ cm^{-3} K^{-1}.

	$\Delta\mu_0H$ = 0–1 T			$\Delta\mu_0H$ = 0–2 T			$\Delta\mu_0H$ = 0–5 T		
Ln	T_{max}	ΔS (mass)	ΔS (volume)	T_{max}	ΔS (mass)	ΔS (volume)	T_{max}	ΔS (mass)	ΔS (volume)
Gd	2	26.72	191.69	2	50.94	365.45	2	69.13	495.95
Tb	4	13.59	98.27	4	21.96	158.75	4	25.65	185.40
Dy	2	12.73	96.30	2	20.75	156.94	3	23.75	179.64
Ho	5	10.15	77.62	6	17.80	136.12	8	21.22	162.25
Er	2	10.29	79.55	2	19.78	152.89	2	25.51	197.19

for magnetic refrigeration over a wide temperature range. The large magnetocaloric effect in these materials is partly due to the high density of the LnF_3 series [7.6441(20) g cm^{-3} for HoF_3 at 300 K] and the large magnetic entropy of the lanthanide ions coupled with their magnetization rapidly increasing at low applied magnetic fields. HoF_3 is an extremely competitive magnetocaloric in a range of applied fields for cooling below 20 K, with potential applications including hydrogen liquefaction. The decrease in $-\Delta S_m$ at low temperatures and the apparent inverse MCE may mean some care in its application is required, but if used for cooling in the 10–20 K range, this complication should be avoided. Therefore, it was desirable to further explore the magnetic behavior on a microscopic level using neutron scattering.

C. Dynamic magneto-structural relationships of HoF_3

Ho^{3+} is a non-Kramers ion, which, in combination with the low site symmetry (C_{1h}), leads to the electronic ground state being a non-magnetic singlet state.[21,37,38] It has previously been reported that a Schottky-type feature associated with transition to this electronic ground state is centered at 3.5 K; however, this is a broad transition, and, as a result, HoF_3 remains paramagnetic well below 1 K.[21,39] HoF_3 magnetically orders at T_N = 0.53 K into a canted antiferromagnetic state, with ferromagnetic nearest neighbor correlations and strong anisotropy along the *a* axis.[39] The moments have been reported to align along the chain direction and canted 66° toward the nearest neighbor.[20]

Polarized inelastic neutron scattering spectra were collected on HoF_3 at 1.5 K as a function of *Q* and energy with the magnetic contribution to the total spectra shown in Fig. 5. The total spectra and nuclear contributions are shown in Figs. S21 and S22. These spectra did not show any indication of long-range magnetic order at 1.5 K at the elastic line, which is consistent with the previous study. No structured magnetic diffuse scattering has been observed as has been shown in other promising Ising-spin magnetocalorics such as $LnODCO_3$ and $Ln(HCO_2)_3$ phases,[11,12,15–17] suggesting a lack of any short-range magnetic order.

Two magnetic excitations are observed in the spectra centered around ~0.59 and ~4.7 meV. These excitations relate to low-lying excitations that have been previously reported to be the energy gap separating a pair of Ising-like electronic states; the ground state singlet and the excited singlet state at 5.90 cm^{-1} (0.73 meV), and another low-lying excitation at 37.99 cm^{-1} (4.71 meV) to another excited singlet state.[39,40] Integration over all *Q* produces the inelastic

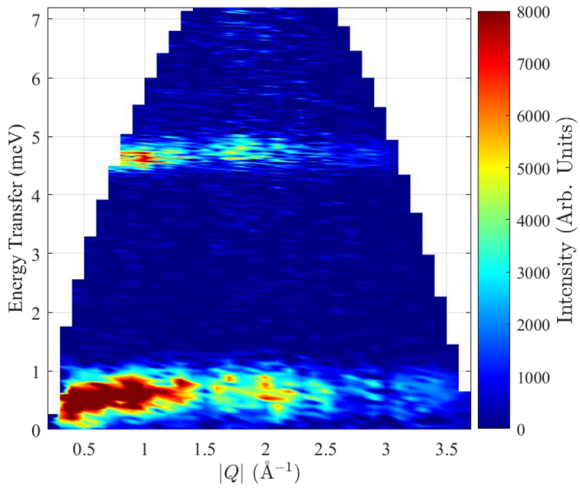

FIG. 5. The normalized magnetic contribution of the inelastic scattering function of HoF_3, separated from the total scattering on D7 by using the XYZ polarization analysis method. There are two clear low-lying excitations centered around 0.59 and 4.7 meV.

scattering function S(ω) shown in Fig. S23. The Gaussian functions have been fit to Fig. S23, and this finds the center of the first excited state to be at 0.589(3) meV, lower in energy than previously reported.[21,39,40] The second excited state was found to be centered at 4.690(4) meV, in very good agreement with previous reports.[21,40] Integration along *Q* of these two excitations is shown in Fig. 6, which shows an increase in the inelastic scattering intensity at low *Q*, indicating that these are not purely point-like transitions, as previously suggested, but are instead non-localized magnetic excitations. The scattering function S(Q) of these excitations is also structured with local maxima in the scattering of both the low and high energy excitations, indicating some order to these dynamical magnetic excitations. The increase in the scattering intensity of the inelastic features with decreasing *Q* is consistent with the presence of ferromagnetic fluctuations in the paramagnetic phase.[41–43]

Bleaney *et al.*[21,39] have previously revealed a low-lying state with a gap of 8.14 cm^{-1} (1.009 meV), which has been attributed to a magnon in the magnetically ordered phase. The fit to the low energy excitation in Fig. S23 results in a δE/E of ~23%, far greater than the expected energy resolution of D7 at this energy,

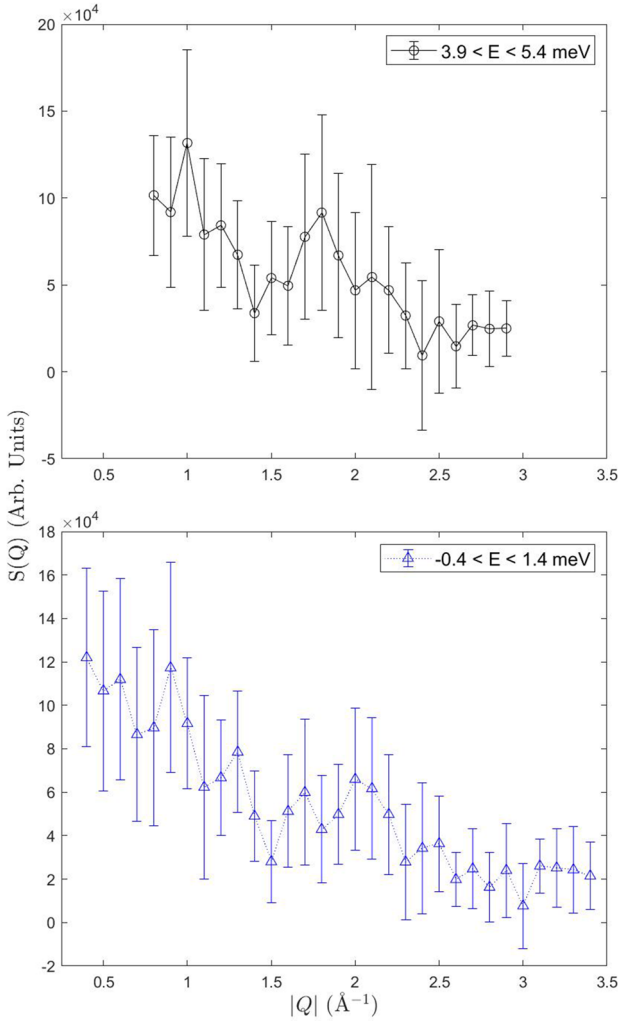

FIG. 6. The magnetic inelastic scattering intensity as a function of momentum transfer S(Q) of the high energy mode (top) and the low energy mode (bottom). The limits of the energy integration windows are listed in the figures.

suggesting the presence of two excitations very close in energy consistent with the previous studies suggesting two excitations at around 0.8–1.0 meV.

To investigate the origin of the low-energy magnetic feature further, the energy of the low-energy excitations has been studied as a function of Q. Figure 7 shows the change in the intensity and energy of the low-energy excitation as a function of Q. At the lowest Q bin ($0.3\ \text{Å}^{-1} < Q < 0.6\ \text{Å}^{-1}$), the excitation is centered at 0.429(8) meV, shifting to higher energies at higher Q bins, up to 0.636(6) meV, where $1.5\ \text{Å}^{-1} < Q < 1.8\ \text{Å}^{-1}$, and shifting to lower energies at the highest Q bins. The changes in energy maxima as a function of Q are a clear indication of a dispersive excitation, providing further

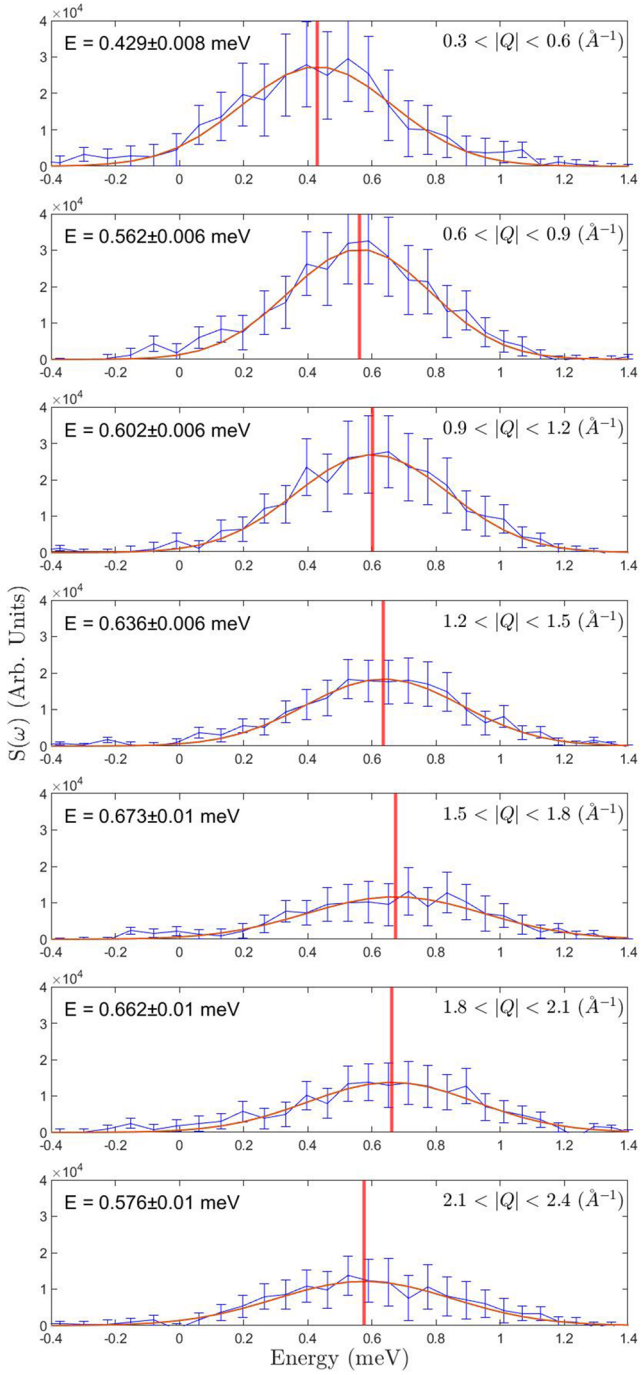

FIG. 7. Comparison of the energy-dependence of the magnetic inelastic scattering from the low-lying excitation, at various Q. The peaks have been fitted with a Gaussian model, shown in red, to extract the peak center indicated by the vertical red line. The peak in energy changes as a function of Q indicating that this mode is weakly dispersive.

evidence that this excitation has a magnetic origin and is an indication of correlations in the dynamic moments in the paramagnetic phase.

Therefore, we would expect that at temperatures below T_N, where the temperature is no longer disrupting correlations, these features may sharpen into a well-defined spin wave. While, qualitatively, the higher energy excitation appears to also be weakly dispersive, the statistics are quite poor and so fits are subject to a high degree of error (see Fig. S24).

Measurements as a function of temperature were performed in the diffraction mode of D7, without the Fermi chopper, so there is no energy analysis. The instrument integrates the scattering over all final neutron energies in this mode, and the attribution of Q is determined based on the scattering angle, 2θ, and the assumption that the scattering is quasielastic. The assumption is known as the static approximation. Figure 5 indicates that all of the magnetic scattering intensity in HoF_3 is inelastic, with significant spectral weight in the higher energy mode, and therefore, absolute Q values obtained using this approximation should be considered tentatively. Figure 8 shows the scattering intensity of HoF_3 in diffraction mode integrated over all final neutron energies. The data appear to show some structure between 1.6 $Å^{-1} < Q < 3.1$ $Å^{-1}$, but this is due to the integration over the inelastic scattering observed in Fig. 5 rather than any structural order. It is unlikely that this structure has any significant contribution from leakage from the nuclear scattering as there is only one peak since there is limited Bragg scattering over this Q-range (cf. Figs. 5 and S22). Differences can be observed between lower and higher temperature polarized neutron patterns. This suggests that the magnetic excitations are changing gradually with temperature.

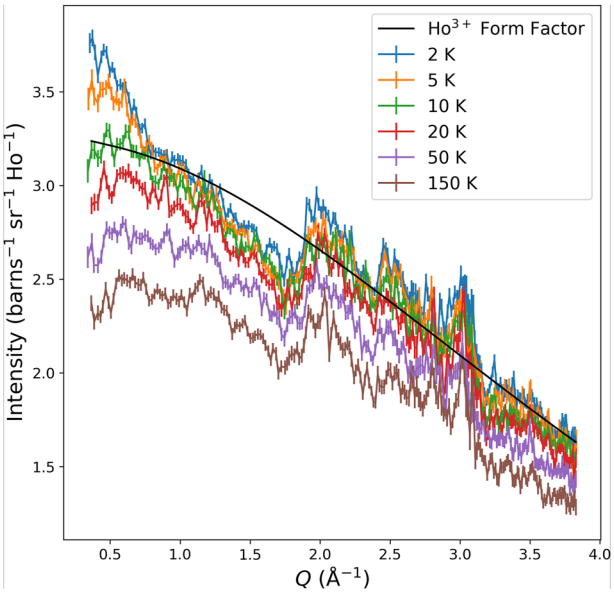

FIG. 8. Comparison of the magnetic scattering measured in the diffraction mode, integrating over all final neutron energies, as a function of temperature between 2 and 150 K. As described in the text, the scattering in the range of ~1.6 $Å^{-1} > Q >$ ~3.1 $Å^{-1}$ is caused by the low-lying excitations and not Bragg peaks from the magnetic structural order.

Specifically, the increase in scattering intensity at low Q indicated by inelastic spectroscopy to arise from ferromagnetic fluctuations at 1.5 K is lost above 10 K. While the dynamical spin fluctuations in HoF_3 are not well described by a purely paramagnetic magnetic form factor, comparison to this in Fig. 8 does highlight this decrease in intensity on heating. It also suggests that above 10 K the magnetic scattering decreases slightly, when approaching $Q = 0$, suggesting the presence of limited antiferromagnetic fluctuations. We interpret these observations as evidence for the existence of ferromagnetic spin fluctuations through the temperatures at which the MCE peaks in HoF_3.[43]

Based on previous studies, combined with our measurements, we can suggest an origin of the interesting magnetocaloric behavior of HoF_3. The decrease in the magnetocaloric effect below 4 K and the apparent significant inverse magnetocaloric effect at 2 K are likely associated with the transition to the singlet ground state, which will decrease the magnetic moment on the Ho^{3+} cation as the temperature decreases. Thus, the magnetization will increase with increasing temperature as the excited states are thermally populated and the Ho^{3+} has a progressively larger magnetic moment. This suggestion is supported by the temperature at which $-\Delta S_m$ first decreases being approximately that of the heat capacity anomaly reported previously at 3.5 K.[21] The remaining magnetic moments order antiferromagnetically at lower temperatures will increase the rate at which magnetization decreases with temperature as this approaches. Inverse MCE is not common but has been previously attributed to crystal field effects, such as in $PrNi_5$,[44] and magnetic ordering, including in $Ba_3Tb(BO_3)_3$ and $Dy(HCO_2)(C_2O_4)$;[5,45] it may be both of these are relevant factors in HoF_3. With respect to the behavior of HoF_3 at higher temperatures, our diffuse magnetic scattering patterns of HoF_3 suggest significant ferromagnetic fluctuations at 5 K, and based on the known magnetic structure, these are likely intrachain correlations. The proximity of the Ho cations in HoF_3 and single fluoride ion separating them leads to the interactions between spins being quite strong with the spins having strong anisotropy along the chain directions.[20] As for other materials with ferromagnetic chains of magnetically anisotropic spins, this will enable the ready alignment of the spins under applied fields, leading to higher $-\Delta S_m$ at low fields.[11,12,15,16,18] Persistence of the significant ferromagnetic intrachain interactions is likely the cause of the gradual decrease in $-\Delta S_m$ compared to other systems in which the cations are packed less densely.

IV. CONCLUSIONS

This work has explored the magnetocaloric effects of the magnetically anisotropic LnF_3 phases, which have highly competitive $-\Delta S_m^{max}$ with respect to volume due to their dense structures. Among these promising materials, HoF_3 is the most interesting, exhibiting considerable conventional MCE above 5 K in low applied fields, which only gradually decreases with temperature such that significant magnetocaloric effects are observed up to 20 K, useful for hydrogen liquefaction. The $-\Delta S_m$ of HoF_3 decreases below 4 K with a possibility of significant inverse MCE at 2 K. Based in part on an examination of HoF_3 with inelastic neutron scattering, the decrease in $-\Delta S_m$ below 4 K is attributed to the singlet ground state of HoF_3 combined with the previously reported antiferromagnetic ordering below 1 K. The promising conventional MCE at tempera-

tures well above 10 K is attributed to the existence of significant 1D ferromagnetic correlations.

SUPPLEMENTARY MATERIALS

See supplementary material for diffraction patterns, additional magnetic properties data, and further neutron spectroscopy data.

ACKNOWLEDGMENTS

R.J.C.D. acknowledges the University of Kent for financial support through the provision of a Vice-Chancellor's scholarship for the initial funding. The authors acknowledge EPSRC for funding this research (Grant Nos. EP/S03577X/1 and EP/T027886/1). The authors would like to thank the Institut Laue Langevin for access to neutron scattering facilities in Grenoble. The authors would like to thank Malte Grosche and Jiasheng Chen from the Cavendish Laboratory, University of Cambridge, for useful discussions.

AUTHOR DECLARATIONS

Conflict of Interest

The authors have no conflicts to disclose.

Author Contributions

All authors contributed to this manuscript. Data collection and analysis, was primarily performed by R.J.C.D. with contributions from P.W.D. and G.B.G.S.. This specific project was conceptualised by R.J.C.D., and this manuscript was written by R.J.C.D. A.W. contributed significantly through data collection, data reduction and supervision of neutron scattering data and analysis. P.J.S. assisted with conceptualising the idea, acquired funding for this project, validated the analysis and contributed to the writing and editing of this manuscript.

Richard J. C. Dixey: Conceptualization (lead); Data curation (lead); Formal analysis (lead); Validation (lead); Visualization (lead); Writing – original draft (lead); Writing – review & editing (equal). **Andrew Wildes**: Data curation (supporting); Supervision (supporting); Writing – review & editing (supporting). **Patrick W. Doheny**: Formal analysis (supporting). **Gavin B. G. Stenning**: Investigation (supporting). **Paul J. Saines**: Conceptualization (supporting); Funding acquisition (lead); Supervision (lead); Validation (equal); Writing – review & editing (equal).

DATA AVAILABILITY

The data that support the findings of this study are available from the corresponding author upon reasonable request.

REFERENCES

[1] O. Sari and M. Balli, Int. J. Refrig. **37**, 8 (2014).
[2] A. Kitanovski, J. Tušek, U. Tomc, U. Plaznik, M. Ožbolt, and A. Poredoš, *Magnetocaloric Energy Conversion* (Springer, 2015).
[3] T. Numazawa, K. Kamiya, T. Utaki, and K. Matsumoto, Cryogenics **62**, 185 (2014).
[4] R. Li, G. Li, and C. Greaves, J. Mater. Chem. A **6**, 5260 (2018).
[5] M. Falsaperna, G. B. G. Stenning, I. da Silva, and P. J. Saines, J. Mater. Chem. C **9**, 13209 (2021).
[6] E. Palacios, J. A. Rodríguez-Velamazán, M. Evangelisti, G. J. McIntyre, G. Lorusso, D. Visser, L. J. De Jongh, and L. A. Butner, Phys. Rev. B **90**, 214423 (2014).
[7] Y.-Z. Zheng, G.-J. Zhou, Z. Zheng, and R. E. P. Winpenny, Chem. Soc. Rev. **43**, 1462 (2014).
[8] Y.-C. Chen, J. Prokleška, W.-J. Xu, J.-L. Liu, J. Liu, W.-X. Zhang, J.-H. Jia, V. Sechovský, and M.-L. Tong, J. Mater. Chem. C **3**, 12206 (2015).
[9] B. Daudin, R. Lagnier, and B. Salce, J. Magn. Magn. Mater. **27**, 315 (1982).
[10] Y. Yang, Q.-C. Zhang, Y.-Y. Pan, L.-S. Long, and L.-S. Zheng, Chem. Commun. **51**, 7317 (2015).
[11] P. J. Saines, J. A. M. Paddison, P. M. M. Thygesen, and M. G. Tucker, Mater. Horiz. **2**, 528 (2015).
[12] R. J. C. Dixey and P. J. Saines, Inorg. Chem. **57**, 12543 (2018).
[13] T. Numazawa, K. Kamiya, T. Okano, and K. Matsumoto, Physica B **329–333**, 1656 (2003).
[14] P. Mukherjee, E. Suard, and S. E. Dutton, J. Phys.: Condens. Matter **29**, 405807 (2017).
[15] R. J. C. Dixey, G. B. G. Stenning, P. Manuel, F. Orlandi, and P. J. Saines, J. Mater. Chem. C **7**, 13111 (2019).
[16] R. J. C. Dixey, F. Orlandi, P. Manuel, P. Mukherjee, S. E. Dutton, and P. J. Saines, Philos. Trans. R. Soc., A **377**, 20190007 (2019).
[17] R. J. C. Dixey, P. Manuel, F. Orlandi, P. Mukherjee, S. E. Dutton, G. B. G. Stenning, and P. J. Saines, J. Mater. Chem. C **8**, 12123 (2020).
[18] D. R. Harcombe, P. G. Welch, P. Manuel, P. J. Saines, and A. L. Goodwin, Phys. Rev. B **94**, 174429 (2016).
[19] M. Piotrowski, H. Ptasiewicz-bąk, and A. Murasik, Phys. Status Solidi A **55**, K163 (1979).
[20] P. J. Brown, J. B. Forsyth, P. C. Hansen, M. J. M. Leask, R. C. C. Ward, and M. R. Wells, J. Phys.: Condens. Matter **2**, 4471 (1990).
[21] B. Bleaney, J. F. Gregg, R. W. Hill, M. Lazzouni, M. J. M. Leask, and M. R. Wells, J. Phys. Colloq. **49**, C8 (1988).
[22] J. Rodríguez-Carvajal, Physica B **192**, 55 (1993).
[23] J. R. Stewart, P. P. Deen, K. H. Andersen, H. Schober, J.-F. Barthélémy, J. M. Hillier, A. P. Murani, and T. Hayes, B. Lindenau, J. Appl. Crystallogr. **42**, 69 (2009).
[24] H. N. Russell and F. A. Saunders, Astrophys. J. **61**, 38 (1925).
[25] L. Holmes and H. J. Guggenheim, J. Phys. Colloq. **32**, C1 (1971).
[26] J. Brinkmann, R. Courths, S. Hüfner, and H. J. Guggenheim, J. Magn. Magn. Mater. **6**, 279 (1977).
[27] P. Mukherjee and S. E. Dutton, Adv. Funct. Mater. **27**, 1701950 (2017).
[28] J. Filippi, F. Tcheou, and J. Rossat-Mignod, Solid State Commun. **33**, 827 (1980).
[29] J. Hammann and M. Ocio, Physica B+C **86–88**, 1153 (1977).
[30] B. L. Reid, D. F. McMorrow, P. W. Mitchell, O. Prakash, and A. P. Murani, Physica B **174**, 51 (1991).
[31] P. J. Saines and N. C. Bristowe, Dalton Trans. **47**, 13257 (2018).
[32] Y. Meng, Y.-C. Chen, Z.-M. Zhang, Z.-J. Lin, and M.-L. Tong, Inorg. Chem. **53**, 9052 (2014).
[33] Y.-C. Chen, L. Qin, Z.-S. Meng, D.-F. Yang, C. Wu, Z. Fu, Y.-Z. Zheng, J.-L. Liu, R. Tarasenko, M. Orendáč, J. Prokleška, V. Sechovský, and M.-L. Tong, J. Mater. Chem. A **2**, 9851 (2014).
[34] H. Zhang, C. Xing, H. Zhou, X. Zheng, X. Miao, L. He, J. Chen, H. Lu, E. Liu, W. Han, H. Zhang, Y. Wang, Y. Long, L. van Eijk, and E. Brück, Acta Mater. **193**, 210 (2020).
[35] P. Mukherjee, A. C. Sackville Hamilton, H. F. J. Glass, and S. E. Dutton, J. Phys.: Condens. Matter **29**, 405808 (2017).
[36] R. Li, P. Manuel, F. Orlandi, and C. Greaves, J. Mater. Chem. A **6**, 21149 (2018).

[37] P. H. E. Meijer, Physica **26**, 61 (1960).
[38] H. A. Kramers, Physica **1**, 182 (1934).
[39] B. Bleaney, J. F. Gregg, R. W. Hill, M. Lazzouni, M. J. M. Leask, and M. R. Wells, J. Phys. C: Solid State Phys. **21**, 2721 (1988).
[40] K. K. Sharma, F. H. Spedding, and D. R. Blinde, Phys. Rev. B **24**, 82 (1981).
[41] Z. Huesges, M. M. Koza, J. P. Embs, T. Fennell, G. Simeoni, C. Geibel, C. Krellner, and O. Stockert, J. Phys.: Conf. Ser. **592**, 012083 (2014).
[42] S. Ramos, E. M. Forgan, C. Bowell, S. M. Hayden, A. J. Schofield, A. Wildes, E. A. Yelland, S. P. Brown, M. Laver, R. S. Perry, and Y. Maeno, Physica B **403**, 1270 (2008).
[43] A. T. Boothroyd, R. Coldea, D. A. Tennant, D. Prabhakaran, L. M. Helme, and C. D. Frost, Phys. Rev. Lett. **92**, 197201 (2004).
[44] P. J. von Ranke, V. K. Pecharsky, K. A. Gschneidner, and B. J. Korte, Phys. Rev. B **58**, 14436 (1998).
[45] N. D. Kelly, C. Liu, and S. E. Dutton, J. Solid State Chem. **292**, 121640 (2020).